 doi:10.20944/preprints202201.0300.v1

Article

Copper Oxide/ Functionalized Graphene Hybrid Nanostructures for Room Temperature Gas Sensing Applications

Monika Gupta [1,2,*], Huzein Fahmi Hawari [1,2,*], Pradeep Kumar [1,2], and Zainal Arif Burhanudin [1,2]

[1]Department of Electrical and Electronic Engineering, Universiti Teknologi PETRONAS, Seri Iskandar 32610, Perak, Malaysia; pradeep.hitesh@gmail.com (P.K.); zainalarif.burhanudin@utp.edu.my (Z.A.B.)
[2] Center of Innovative Nanostructures and Nanodevices (COINN), Universiti Teknologi PETRONAS, Seri Iskandar 32610, Perak, Malaysia
*Correspondence: monika_18000995@utp.edu.my (M.G.); huzeinfahmi.hawari@utp.edu.my (H.F.H.)

Abstract: Oxide semiconductors are conventionally being used as sensing materials in gas sensors, limiting the detection of gases at room temperature (RT). In this work, a hybrid of copper oxide (CuO) with functionalized graphene (rGO) is proposed to achieve gas sensing at RT. The combination of high surface area and presence of many functional groups in CuO/rGO hybrid material makes it highly sensitive for gas absorption and desorption. To prepare the hybrid material, a copper oxide suspension synthesized using copper acetate precursor is added to the graphene oxide solution during its reduction using ascorbic acid. Material properties of CuO/rGO hybrid and its drop-casted thin films are investigated using Raman, FTIR, SEM, TEM, and four-point probe measurement systems. We find that the hybrid material is enriched with oxygen functional groups (OFGs) and defective sites along with electrical conductivity (~1.5 kΩ/□). The fabricated QCM (quartz crystal microbalance) sensor with a thin layer of CuO/rGO hybrid, demonstrates a high sensing response which is twice the response of the rGO-based sensor for CO_2 gas at RT. We believe that the CuO/rGO hybrid can be highly suitable for existing and future gas sensors used for domestic and industrial safety.

Keywords: Sensing materials, CuO/rGO hybrid, graphene, QCM, gas sensor, room temperature sensing.

1. Introduction

Over the past few decades, the environment is heavily filled with toxic, inflammable, and harmful gases due to the unceasing development of industries and deforestation [1]. The level of these gases is excessively increased in the atmosphere after industrialization. For a safe and healthy environment, the detection of these gases is seriously demanded [2–4]. The need for an effective gas sensor is then extremely important. Numerous gas sensors based on the IDE (interdigitated electrode) [5–7], FET (field-effect transistor) [8,9], MEMS (microelectromechanical systems) [10,11], and QCM [12–14] have been developed. Among them, the QCM-based gas sensor is very effective owing to its attractive features such as accuracy, high sensitivity, and fast response. Also, QCM can be easily integrated with other electronic components [15,16].

In these gas sensors, metal oxide semiconductors such as zinc oxide (ZnO) [17], nickel oxide (NiO) [18], Tin oxide (SnO_2) [19,20], titanium dioxide (TiO_2) [21], and copper oxide (CuO) [22] have been fabricated and used as the sensing materials. Among numerous metal oxide semiconductors, CuO has gained more attention due to its low cost, non-toxicity, facile preparation, and high surface reactivity [23,24]. CuO is a p-type

Preprints (www.preprints.org) | NOT PEER-REVIEWED | Posted: 20 January 2022 doi:10.20944/preprints202201.0300.v1

semiconductor and has a narrow bandgap of 1.2–1.9 eV and exhibits excellent properties that have been utilized in a number of applications such as electrode materials for lithium-ion batteries, thin-film electrodes [25], catalysts [21], and gas sensors [26]. However, these CuO sensing materials need a high temperature to operate, which limits the gas sensing at room temperature.

The incorporation of CuO with carbon-based materials can be an effective approach to realize reliable gas sensors at room temperature (RT). Carbon-based two-dimensional (2D) material like graphene has outstanding electronic, mechanical, and thermal properties as well as a large surface-to-volume ratio [27–29]. Graphene has been used as a sensing material for RT detection of various gases such as nitrogen dioxide (NO_2), sulfur dioxide (H_2S), ammonia (NH_3), and hydrogen (H_2) [30–33]. But lower electrical conductivity of graphene thin films also limits their sensors to achieve high performance.

Here, we report CuO/ functionalized graphene (rGO) hybrid nanostructure as a promising sensing material for QCM-based sensors for detecting the gas at room temperature. In synthesis, initially, the CuO nanoparticles (NPs) are prepared using copper acetate as a precursor and then mixed with functionalized graphene oxide solution. The functionalized graphene oxide is achieved using the chemical reduction method by ascorbic acid. The sensing thin films of the synthesized hybrid material are developed by the drop-cast method. The synergistic effect of CuO and graphene in the hybrid structure can help to achieve the detection of gas at room temperature. The CuO/rGO hybrid offers tremendous properties such as enhanced surface reactivity, good electrical conductivity, and large surface area. The CuO/rGO hybrid and rGO-based gas sensors are prepared to investigate the CO_2 gas sensing at room temperature.

2. Materials and Methods

2.1 Materials

Graphene oxide (GO) paste (95%) was purchased from Graphenea (San Sebastian, Spain). Ascorbic acid, ethanol (95%), and acetone (95%) were purchased from Sigma Aldrich (St. Louis, MO, USA). Copper acetate (99.9% purity), hexamethylenetetramine, and isopropyl alcohol (IPA, 99.9% purity) were bought from R & M Chemicals. All the chemicals were of analytical grade, no further purification was required for conducting experiments. Deionized (DI) water was used in all preparations.

2.1 Synthesis of CuO/ Functionalized Graphene Hybrid and Thin Film Development

The schematic representation of CuO/rGO hybrid synthesis is shown in scheme 1. Initially, 4 g of copper acetate is added to 60 ml IPA and mixed under the stirring condition at 80 °C for 20 min. Then, 4ml of ethanolamine (MEA) is added carefully to the solution and stirred vigorously for 2 h. The prepared solution is left for 24 hrs for aging. The solution is further washed with water and the solid product was separated using centrifugation. Next, 30 ml Graphene oxide (0.5 mg/ml) was dissolved in 100.00 mL of DI water and vigorously stirred for 10 min to form a well-mixed suspension. Then, 100

Preprints (www.preprints.org) | NOT PEER-REVIEWED | Posted: 20 January 2022 doi:10.20944/preprints202201.0300.v1

mg ascorbic acid (AA) is carefully added to the suspension. Afterward, 0.02 g of obtained CuO powder is added immediately to this GO suspension followed by vigorous stirring at 80 °C for 4 hrs. The suspension is further washed with ethanol and water (1:1 ratio). The solid product was later collected after the centrifugation followed by drying in the oven at 60 °C.

For comparison, the rGO is also synthesized using our previous work [34]. In brief, 15 ml of GO was added in 30 ml of DI water followed by ultrasonication for 15 min to acquire a uniform aqueous dispersion. Then, 100 mg of ascorbic acid was carefully added to the GO suspension, then stirred for 1 h at 65 ºC under RT environment conditions. The change in color of GO suspension from brown to black suggested the accomplishment of functionalized graphene oxide.

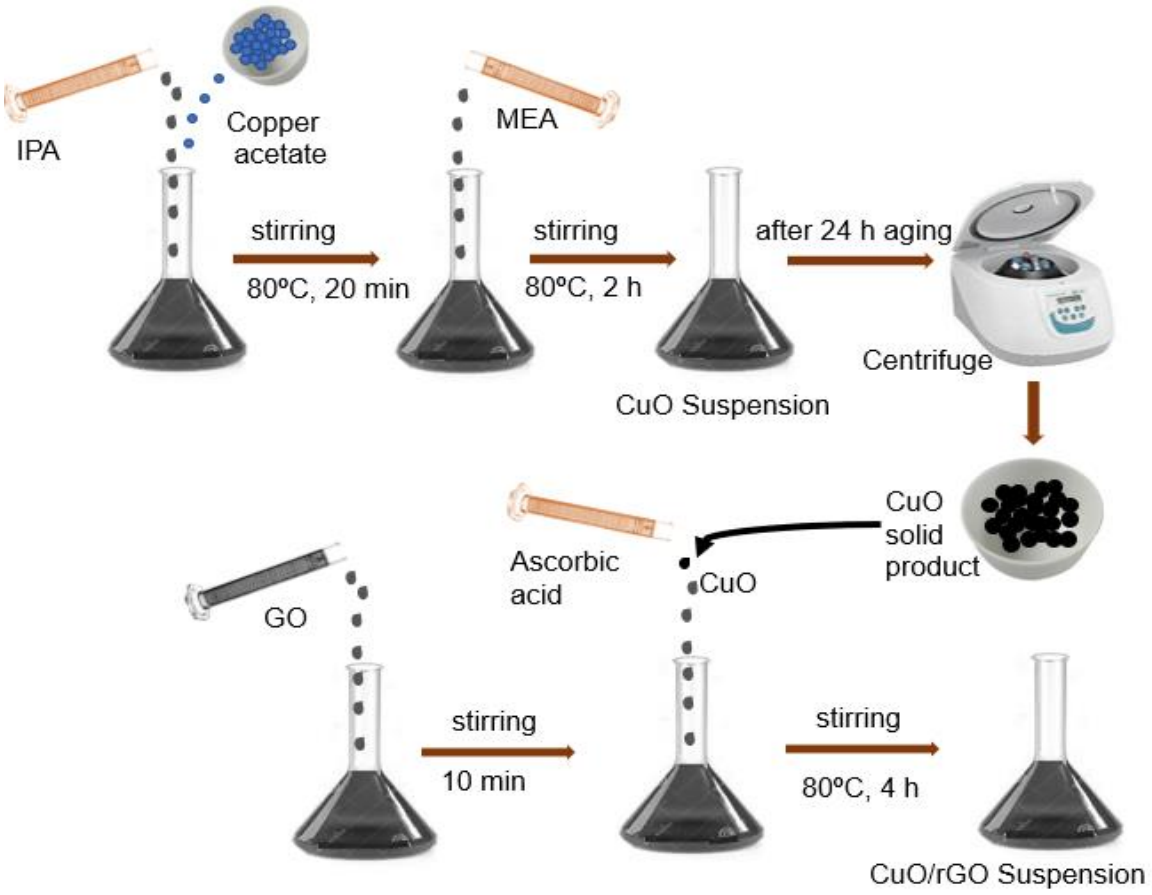

Scheme 1. Schematic representation of CuO/functionalized graphene (rGO) hybrid synthesis.

The thin films of synthesized rGO suspensions and CuO/rGO hybrid were developed by the drop-casting method. Before thin-film development, the target substrates such as glass and SiO_2 (300 nm)/Si were washed in acetone, isopropyl alcohol, DI water, and ethanol using ultrasonication for 15 min in each solvent.

For sensor fabrication, thin sensing layers of CuO/rGO hybrid and rGO materials were drop casted on a silver (Ag) electrode of 10 MHz QCM (WTL International China, Shenzhen, China). Before that, the QCM resonators were cleaned properly using acetone, isopropyl alcohol (IPA), DI water, and ethanol. A custom-made QCM based gas sensing

Preprints (www.preprints.org) | NOT PEER-REVIEWED | Posted: 20 January 2022 doi:10.20944/preprints202201.0300.v1

setup is used to get the sensing performance. Before sensing the rGO and CuO/rGO coated QCM were dried at room temperature.

2.2 Characterization

The structural and morphological properties of synthesized materials were investigated by Fourier Transform Infrared (FTIR) spectroscopy (Bruker Instruments, model Aquinox 55, Stuttgart), Raman spectroscopy (Horiba Jobin Yvon HR800, Yvon, France, 514 nm laser excitation) for 200 to 4000 cm^{-1} spectrum regions, and Transmission electron microscopy (TEM, Zeiss Libra 200FE, Jena, Germany), respectively. The sheet resistance of thin films of prepared materials was measured using a four-point probe measurement system (Lucas Lab 302) with Keithley 2400 source meter.

For gas sensing, rGO and CuO/rGO hybrid coated QCMs were placed inside the QCM holder. In the typical arrangement, the QCM holder is connected to the frequency counter. When gas is pursed to QCM sensors, the analyte gas molecules get absorbed at the material surface and the frequency of QCM gets changed. The frequency counter counts the frequency change. The response and recovery curve can be observed in the attached computer. The sensitivity (S) can be calculated using equation (10) [13],

$$S = \frac{Frequency\ shift\ (Hz)}{amount\ of\ material\ coated\ on\ QCM\ electrode\ (\mu g)} \quad (1)$$

3. Results and Discussion

3.1. FTIR Analysis

FTIR spectrum is used to identify the presence of functional groups and chemical compounds. The FTIR spectra of GO, rGO, and CuO/rGO hybrid are shown in Figure 1. The FTIR spectrum of GO exhibited strong peaks at 3182 cm^{-1}, 1620 cm^{-1}, and 1044 cm^{-1}, attributing to the stretching and deformation of -OH and -COOH functional groups as well as the adsorbed and inhibited water molecules to atmospheric moisture [35,36]. The peaks at 1724 cm^{-1} and 1620 cm^{-1} ascribe to the vibrations of C=O stretching and C=C alkene groups stretching vibrations. Some other peaks at 1225 cm^{-1} and 1044 cm^{-1} were also observed, indicating the presence of C-O stretching vibration of epoxy groups and alkoxy group, respectively. Also, in the rGO spectra, weak peaks at 2322 cm^{-1}, and 1391 cm^{-1} were observed possibly due to the stretching and deformation of O-H groups and adsorbed water molecules. The spectrum of rGO also indicated the presence of the stretching vibration bands for C=O at 1717 cm^{-1} and C-O for epoxy and alkoxy at 1219 cm^{-1} and 1007 cm^{-1} respectively.

After the formation of the CuO/rGO hybrid, the peaks for the functional group were found to be shifted to 3198 cm^{-1} (hydroxyl), 1570 cm^{-1} (carboxyl), and 1023 cm^{-1} (epoxy). This suggests the oxygen functional groups (OFGs) particularly hydroxyls have emerged during the formation of a hybrid nanostructure. However, a weak peak for hydroxyls was found in the rGO nanostructure. In CuO/rGO hybrid spectrum, some additional peaks at 560 cm^{-1}, 576 cm^{-1}, and 607 cm^{-1} were also observed, signifying the

Preprints (www.preprints.org) | NOT PEER-REVIEWED | Posted: 20 January 2022 doi:10.20944/preprints202201.0300.v1

vibrations of the Cu–O bond [37]. The presence of these peaks is also attributed to the stabilization of CuO nanoparticles through the residual OFGs present in rGO and shows the presence of copper nanoparticles along with rGO [38].

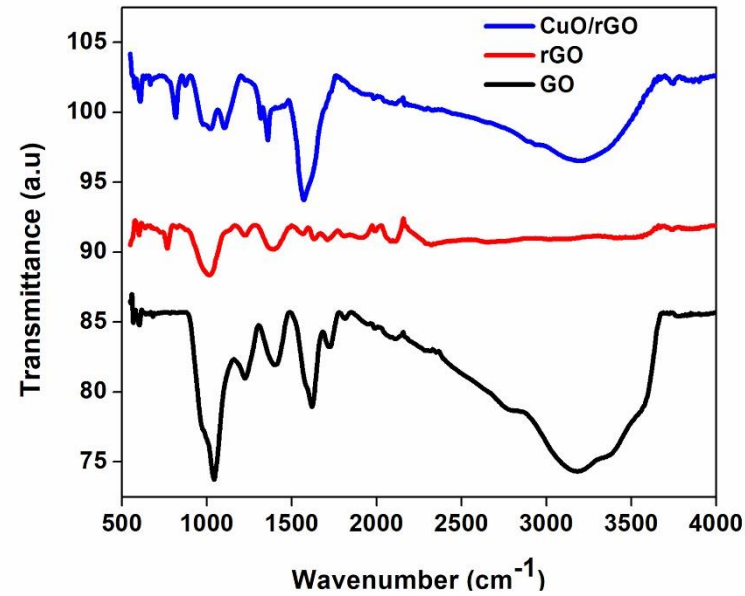

Figure 1. FTIR spectra of GO, rGO, and CuO/rGO hybrid.

3.2 Raman Analysis

Raman spectrum of CuO/rGO hybrid is presented in Figure 2 and compared with spectra of GO, and rGO. The D-peaks for GO, rGO, and CuO/rGO hybrid were found at the Raman shift of ~1355 cm^{-1}, ~1353 cm^{-1}, and 1350 cm^{-1} respectively. The G-peaks for GO, rGO, and CuO/rGO hybrid were observed at the Raman shift of ~1586 cm^{-1}, 1600 cm^{-1}, and 1594 cm^{-1} respectively (see figure 3(a)). Typically, the D-peak appears from the defects in sp^3 carbon atoms whereas G-peak correlates to the sp^2 carbon atoms [39,40]. The prepared rGO and CuO/rGO material inhibit intense D-peak and G-peak, which is attributed to the presence of defects in the graphene layer. The D-peak of rGO and CuO/rGO hybrid was observed to be more intense as compared to G-peak, indicating the formation of sp^3 graphitic domains and the formation of new defects in the structure during the reduction process [35,41]. The occurrence of two additional peaks at low-frequency Raman shift ~322 cm^{-1} and ~678 cm^{-1}, indicates the A_g and B_g modes of

Preprints (www.preprints.org) | NOT PEER-REVIEWED | Posted: 20 January 2022 doi:10.20944/preprints202201.0300.v1

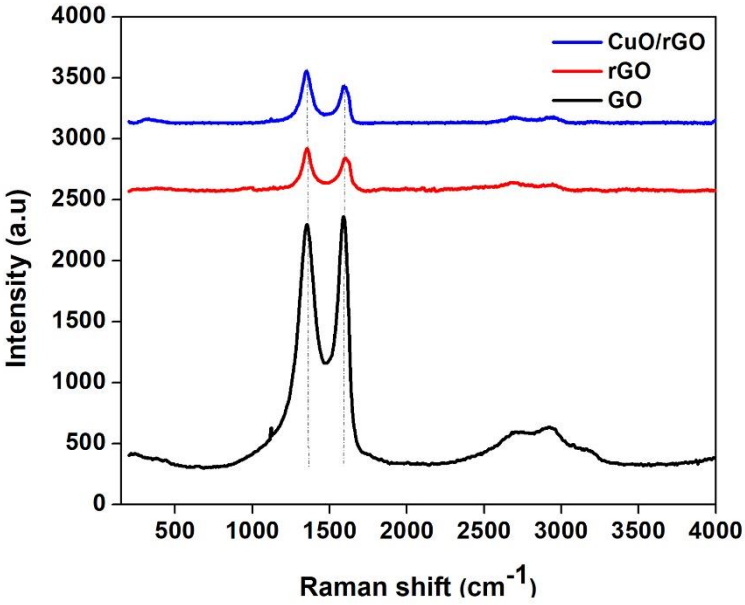

Figure 2. Raman spectra of CuO/rGO hybrid, rGO, and GO.

the vibration of CuO [42]. The 2D peaks were observed at ~2679cm^{-1}, ~2689 cm^{-1}, and ~2701 cm^{-1} for GO, rGO, and CuO/rGO hybrid, respectively. The 2D-band also known as G'-band, originates from the second-order mode of the D-band [43]. The higher wavenumber position and the lowest peak height of the 2D-band of CuO/rGO hybrid suggest the existence of more number of graphene layers as compared to rGO. Moreover, it expresses that the Cu nanoparticles located between graphene layers, work as a spacer to hinder the agglomeration of graphene layers.

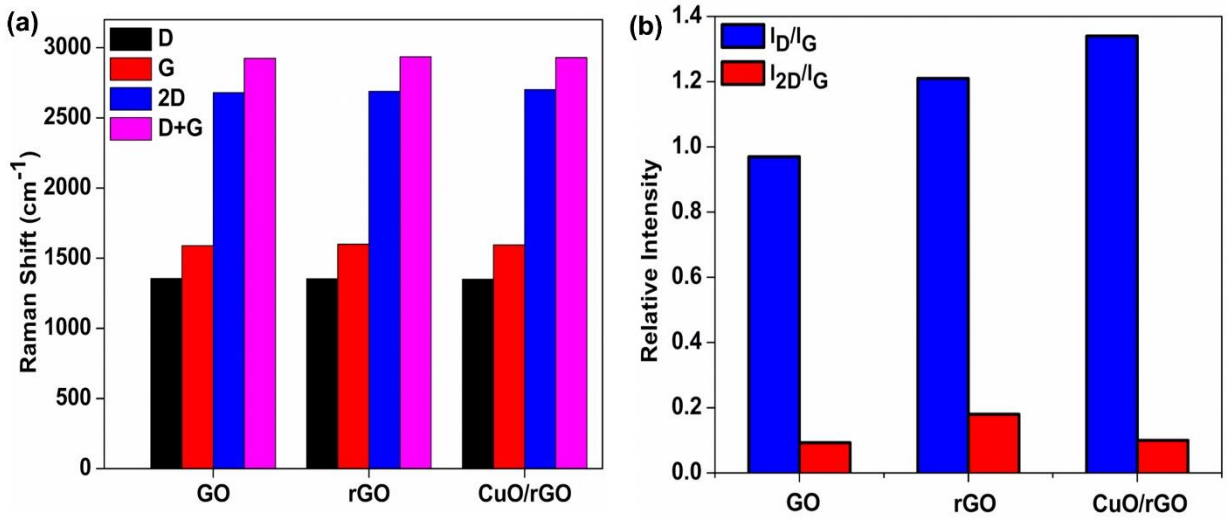

Figure 3. Raman fingerprints- (a) position of D-, G-, 2D-, and D+G – peaks, (b) average values of the parameters I_D/I_G, I_{2D}/I_G obtained from Raman Spectra of rGO and CuO/rGO hybrid.

The I_D/I_G intensity ratio (see Figure 3(b)) was found to be 0.97, 1.21, and 1.35 for GO, rGO, and CuO/rGO hybrid, respectively. I_D/I_G ratio represents the quality or disorder level of graphene. The relatively higher value of I_D/I_G for CuO/rGO hybrid suggests the

Preprints (www.preprints.org) | NOT PEER-REVIEWED | Posted: 20 January 2022 doi:10.20944/preprints202201.0300.v1

formation of higher graphitic domains (smaller spatial dimensions) [44]. This indicates a decrease in the average size of the sp^2 carbon domain upon the reduction of GO. Similar results are also reported by Cheng et al. [45]. The higher intensity of D-peak shows the presence of a large amount of OFGs that are favorable for the physisorption of analyte gas molecules. Reduced graphene oxide consists of graphene layers and OFGs attached at its basal plane and edges [35]. The I_{2D}/I_G ratios for GO, rGO, and CuO/rGO hybrid were found to be 0.093, 0.18, and 0.13 indicating the presence of few layers of graphene in the CuO/rGO hybrid.

The deconvoluted Raman spectra (Lorentz fit) of GO, rGO, and CuO/rGO hybrid are shown in Figure 4. The height of the D band, G band, 2D band, and D+G band is shown in Table 1. It was observed that the intensity of the D-peak of rGO and hybrid were lower than the D-peak of GO, attributing to the presence of fewer OFGs in the rGO and hybrid material. Also, the intensity of G-peak was found to be lower than that of D-peak in rGO and hybrid material, showing that these materials have higher defects [46,47].

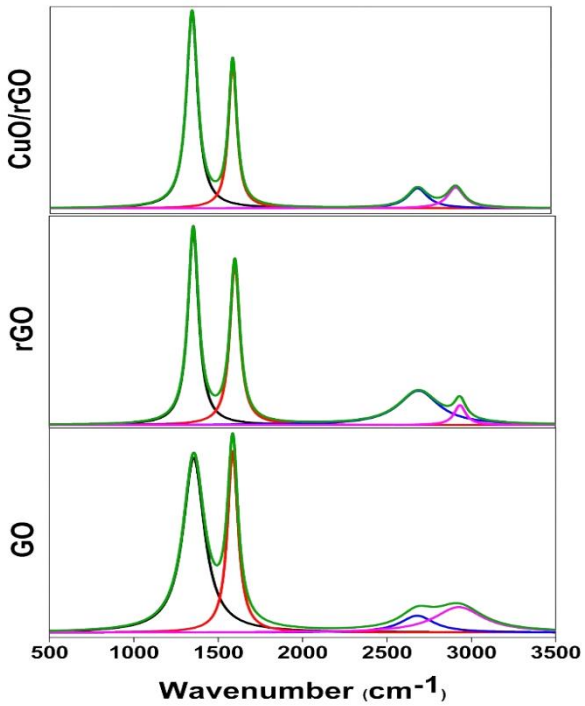

Figure 4. Deconvoluted (Lorentz fit) Raman curve of GO, rGO, and CuO/rGO hybrid.

Full width half maximum (FWHM) values of D- and G-peaks of GO, rGO, and CuO/rGO hybrid are shown in Table 2. A lower value of FWHM of D and G band for CuO/rGO hybrid (~81 cm^{-1} and ~60 cm^{-1}) and rGO (~76 cm^{-1} and 288 cm^{-1}) in comparison to GO (~153 cm^{-1} and 75 cm^{-1}) indicates the presence of fewer OFGs in their structures.

Table 1. Intensity (a.u.) of the bands in the Raman spectra of GO, rGO, and CuO/rGO Hybrid.

Sample	D Band	G Band	2D band	D+G
GO	1877	1947	181	273
rGO	321	265	48	32

Preprints (www.preprints.org) | NOT PEER-REVIEWED | Posted: 20 January 2022 doi:10.20944/preprints202201.0300.v1

CuO/rGO	411	305	41	43

Table 2. FWHM (cm^{-1}) values of the bands in Raman spectra of GO, rGO, and CuO/rGO Hybrid.

Sample	D Band	G Band	2D band	D+G
GO	153	75	241	350
rGO	76	288	82	82
CuO/rGO	81	60	146	120

3.3 SEM and *TEM Analysis*

The structure and morphology of the synthesized materials can be studied using SEM and TEM. Figure 5(a) shows the SEM image of rGO, which consists of wrinkles on its surface. Figure 5(b) shows the surface of the CuO/rGO hybrid, wherein the CuO NPs are distributed throughout the graphene sheets.

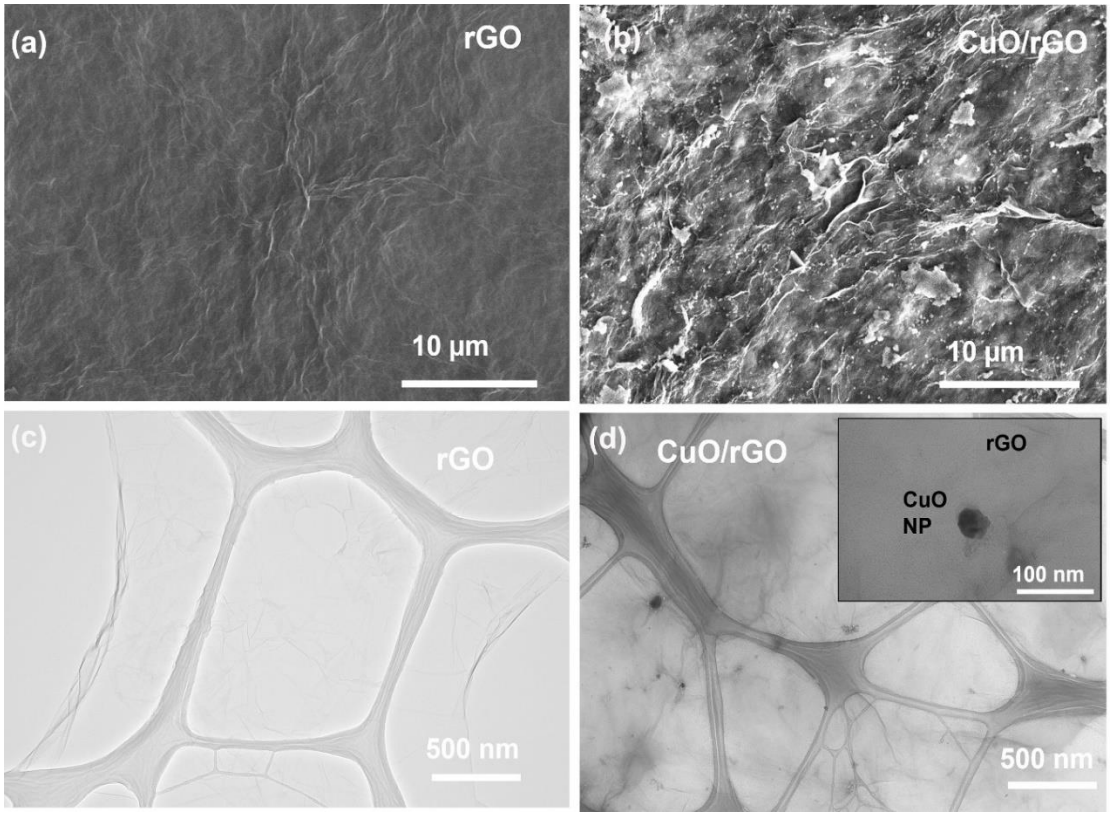

Figure 5. SEM image of (a) rGO and (b) CuO/rGO hybrid, TEM images of (c) rGO and (d) CuO/rGO hybrid. A high-resolution image of the hybrid is shown in the inset.

Figure 5(c) shows the TEM-based rGO morphology. The surface of rGO was identified as a continuous thin layer with few folds and wrinkles on the edges of rGO sheets. Figure 5(d) shows the surface morphology of the CuO/rGO hybrid wherein, the CuO in the form of nanoparticles were well-mixed with rGO. The size (diameter) of CuO particles was observed in the range of 10-40 nm. The CuO nanoparticles were observed

Preprints (www.preprints.org) | NOT PEER-REVIEWED | Posted: 20 January 2022 doi:10.20944/preprints202201.0300.v1

to be randomly distributed on the basal plane of rGO sheets, providing enough surface contact for charge transport. The inset shows the high-resolution image of the CuO/rGO hybrid, displaying the 35 nm CuO nanoparticles on the rGO sheets.

a. Electrical Analysis

Figure 6 shows the sheet resistance (R_S)of the rGO and CuO/rGO hybrid thin films. To investigate the electrical properties of materials four-point probe technique has been used. The electrical characterization is carried out at room temperature. R_S of rGO and CuO/rGO hybrid was found to be 1.85 ± 0.12 kΩ/□ and 1.665 ± 0.11 kΩ/□, respectively. The lower sheet resistance of hybrid is probably due to the presence of CuO nanoparticles.

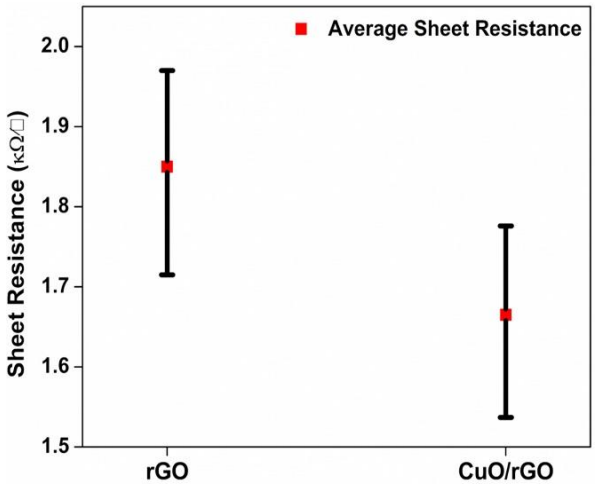

Figure 6. The sheet resistance of rGO, and CuO/rGO hybrid thin films.

3.4 Gas Sensing *Performance*

Figure 7(a) shows the response and recovery curve of rGO/CuO hybrid thin film-based QCM gas sensors for 500 ppm CO_2 at room temperature. A frequency shift (Δf) of 438 Hz was shown by the gas sensor with rGO/CuO hybrid sensing thin-film whereas, Δf of 193 Hz was demonstrated by rGO thin film-based sensor. The higher response of hybrid sensing film is possibly due to the presence of more OFGs at its surface as indicated by FTIR spectra. The CO_2 gas was also exposed to GO coated QCM sensor at RT. The prepared GO coated QCM sensor showed no response upon CO_2 gas exposure possibly due to the unavailability of active sites on its surface. GO has mainly hydroxyl and epoxide groups at its basal plane and it loses sp^2 hybridization during the oxidation process which makes GO an insulating material at room temperature [35].

The comparison between response time, recovery time, and sensitivity of rGO and CuO/rGO hybrid-based gas sensors is presented in Figure 7(b). The response time (T_{res}) was observed to be 43 s and 48 s for CuO/rGO hybrid and rGO thin film-based sensors, respectively, for 500 ppm CO_2 gas at RT. The recovery time of hybrid and rGO-based sensors was observed to be 24 s and 21 s, respectively. The CuO/rGO hybrid–based sensor showed more recovery time than that of the rGO-based sensor. It is possibly due

Preprints (www.preprints.org) | NOT PEER-REVIEWED | Posted: 20 January 2022 doi:10.20944/preprints202201.0300.v1

to the formation of hydroxyl groups. The gas sensing characteristics, frequency shift, response time, and recovery time strongly depend on the interactions between the oxygen functional group (OFGs) and analyte gas molecule [12,48]. The hybrid requires a higher time to recover due to the formation of hydroxyl bonds. Hydroxyl bonds are mainly attached to the basal plane however carboxyl and carbonyls are mainly attached to the edge plane of graphene [35]. These hydroxyls work as trap charges for the analyte gas molecule. Although the rGO and CuO/rGO hybrid thin film-based sensors showed a good response towards CO_2 gas, both sensors demonstrated baseline drift because the adsorbed CO_2 molecules do not desorb completely during the desorption process. The calculated sensitivity of hybrid and rGO–based gas sensors was found to be 15 Hz/μg and 1 Hz/μg for 500 ppm of CO_2 gas.

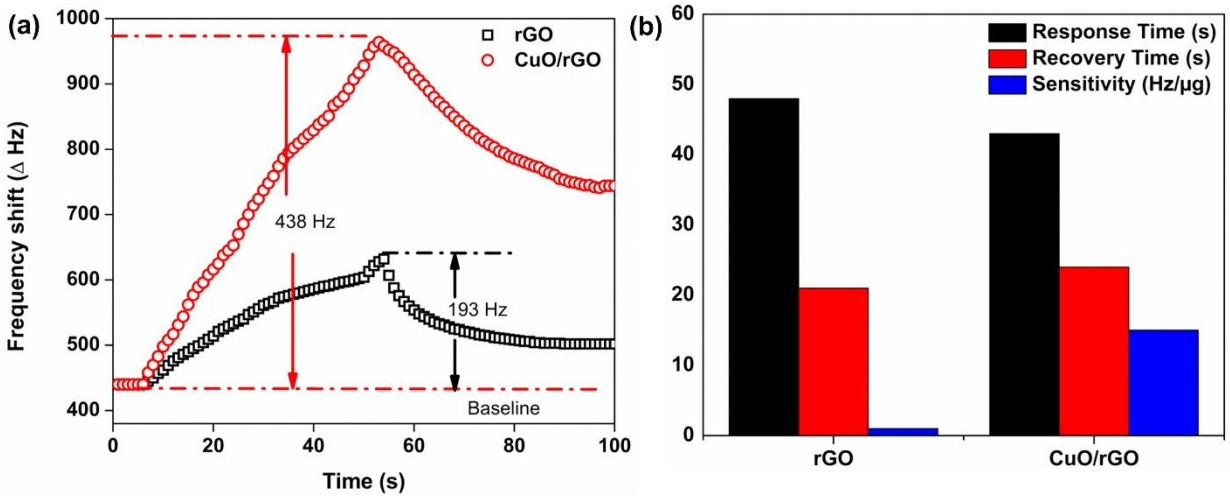

Figure 7. (a) Sensing response curve and (b) comparisons of response time (s), recovery time (s), and sensitivity (Hz/μg) of rGO and CuO/rGO hybrid-based gas sensors.

4. Conclusion

In this work, we have successfully synthesized the CuO/functionalized graphene hybrid material. The thin films of material were developed by the drop-casting method on the substrates. The material properties were examined using advanced spectroscopy and microscopy. In hybrid nanostructure, a wrinkled and folded graphene surface with randomly distributed CuO NPs of size 10-40 nm was observed. The hybrid material was also found to have a large amount of OFGs and defective sites on its surface. The electrical conductivity of CuO/rGO hybrid thin film was measured to be ~1.5 kΩ/□. The functionality of the CuO/rGO hybrid was investigated as a sensing layer in the QCM sensor for gas detection at room temperature. The CuO/rGO hybrid-based gas sensor realized a high sensing response (Δf ~440 Hz, T_{res} ~43 s) for 500 ppm CO_2 gas at room temperature. The sensing performance of the CuO/rGO hybrid-based gas sensor was compared with that of the rGO-based sensor. A 2-fold improved sensing response was achieved in comparison to the rGO-based sensor. The selectivity of the CuO/rGO hybrid

will be investigated in our upcoming work. This study shows the interesting possibilities of CuO/rGO hybrids in future gas sensing devices.

Author Contributions: Conceptualization, M.G. and H.F.H.; methodology, M.G. and P.K.; software, M.G.; formal analysis, M.G. and P.K.; investigation, M.G. and P.K.; resources, H.F.H.; data curation, M.G.; writing—original draft preparation, M.G.; writing—review and editing, P.K., and H.F.H.; visualization, M.G., P.K., and H.F.H.; supervision, H.F.H., and Z.A.B.; project administration, H.F.H.; funding acquisition, H.F.H. All authors have read and agreed to the published version of the manuscript.

Funding: This research was funded by Yayasan Universiti Teknologi PETRONAS (YUTP) grant (number: 015LC0-153). The publication charge was partially supported by the Center for Graduate Studies (CGS), UTP, Malaysia.

Data Availability Statement: The data are available upon request from the corresponding authors.

Acknowledgments: The authors would like to thank the graduate assistantship scheme from the CGS, UTP, Malaysia.

Conflicts of Interest: The authors declare no conflict of interest.

References

1. Leghrib, R. Design, Fabrication and Characterisation of Gas Sensors Based on Nanohybrid Materials, 2011.
2. Azuma, K.; Kagi, N.; Yanagi, U.; Osawa, H. Effects of low-level inhalation exposure to carbon dioxide in indoor environments: A short review on human health and psychomotor performance. *Environ. Int.* **2018**, *121*, 51–56.
3. Yu, B.F.; Hu, Z.B.; Liu, M.; Yang, H.L.; Kong, Q.X.; Liu, Y.H. Review of research on air-conditioning systems and indoor air quality control for human health. *Int. J. Refrig.* **2009**, *32*, 3–20, doi:10.1016/j.ijrefrig.2008.05.004.
4. Tanvir, N.B.; Yurchenko, O.; Wilbertz, C.; Urban, G. Investigation of CO2 reaction with copper oxide nanoparticles for room temperature gas sensing. *J. Mater. Chem. A* **2016**, *4*, 5294–5302, doi:10.1039/c5ta09089j.
5. Rathi, K.; Pal, K. Ruthenium decorated tungsten disulfide quantum dots for CO2 gas sensor. *Nanot* **2019**, *31*.
6. Daud, A.I.; Wahid, K.A.A.; Khairul, W.M. Room-temperature operated cyano-terminated ethynylated-thiourea as a resistive-type carbon dioxide (CO2) gas sensor. *Org. Electron.* **2019**, *70*, 32–41.
7. Young, S.-J.; Lin, Z.-D. Sensing Performance of Carbon Dioxide Gas Sensors with Carbon Nanotubes on Plastic Substrate. *ECS J. Solid State Sci. Technol.* **2017**, *6*, 72–74.
8. Cui, S.; Pu, H.; Wells, S.A.; Wen, Z.; Mao, S.; Chang, J.; Hersam, M.C.; Chen, J. Ultrahigh sensitivity and layer-dependent sensing performance of phosphorene-based gas sensors. *Nat. Commun.* **2015**, *6*, 1–9.
9. Zhang, M.; Brooks, L.L.; Chartuprayoon, N.; Bosze, W.; Choa, Y.H.; Myung, N. V. Palladium/single-walled carbon nanotube back-to-back schottky contact-based hydrogen sensors and their sensing mechanism. *ACS Appl. Mater. Interfaces* **2014**, *6*, 319–326, doi:10.1021/am404328g.
10. Zia, A.I.; Syaifudin, A.R.M.; Mukhopadhyay, S.C.; Yu, P.L.; Al-Bahadly, I.H.; Gooneratne, C.P.; Kosel, J.; Liao, T.S. Electrochemical impedance spectroscopy based MEMS sensors for phthalates detection in water and juices. *J. Phys. Conf. Ser.* **2013**, *439*, doi:10.1088/1742-6596/439/1/012026.
11. Algamili, A.S.; Khir, M.H.M.; Dennis, J.O.; Ahmed, A.Y.; Alabsi, S.S.; Ba Hashwan, S.S.; Junaid, M.M. A Review of Actuation and Sensing Mechanisms in MEMS-Based Sensor Devices. *Nanoscale Res. Lett.* **2021**, *16*, doi:10.1186/s11671-021-03481-7.
12. Berouaken, M.; Talbi, L.; Alkama, R.; Sam, S.; Menari, H.; Chebout, K.; Manseri, A.; Boucheham, A.; Gabouze, N. Quartz Crystal Microbalance Coated with Vanadium Oxide Thin Film for CO 2 Gas Sensor at Room Temperature. *Arab. J. Sci. Eng.* **2018**, *43*, 5957–5963.
13. Yang, M.; He, J.; Hu, X.; Yan, C.; Cheng, Z. CuO nanostructures as quartz crystal microbalance sensing layers for detection of trace hydrogen cyanide gas. *Environ. Sci. Technol.* **2011**, *45*, 6088–6094, doi:10.1021/es201121w.
14. Vashist, S.K.; Vashist, P. Recent advances in quartz crystal microbalance-based sensors. *J. Sensors* **2011**, *2011*.
15. Varga, M.; Laposa, A.; Kulha, P.; Kroutil, J.; Husak, M.; Kromka, A. Quartz crystal microbalance gas sensor with nanocrystalline diamond sensitive layer. *Phys. Status Solidi Basic Res.* **2015**, *252*, 2591–2597.

16. Gupta, M.; Athirah, N.; Hawari, H.F. Graphene derivative coated QCM-based gas sensor for volatile organic compound (VOC) detection at room temperature. *Indones. J. Electr. Eng. Comput. Sci.* **2020**, *18*, 1279–1286, doi:10.11591/ijeecs.v18.i3.pp1279-1286.
17. Zhu, B.L.; Xie, C.S.; Wang, W.Y.; Huang, K.J.; Hu, J.H. Improvement in gas sensitivity of ZnO thick film to volatile organic compounds (VOCs) by adding TiO2. *Mater. Lett.* **2004**, *58*, 624–629, doi:10.1016/S0167-577X(03)00582-2.
18. Ren, H.; Gu, C.; Joo, S.W.; Zhao, J.; Sun, Y.; Huang, J. Effective hydrogen gas sensor based on NiO@rGO nanocomposite. *Sensors Actuators B Chem.* **2018**, *266*, 506–513, doi:10.1016/j.snb.2018.03.130.
19. Chen, W.; Zhou, Q.; Wan, F.; Gao, T. Gas sensing properties and mechanism of Nano-SnO2-based sensor for hydrogen and carbon monoxide. *J. Nanomater.* **2012**, *2012*, doi:10.1155/2012/612420.
20. Lee, Z.Y.; Hawari, H.F. Bin; Djaswadi, G.W. Bin; Kamarudin, K. A highly sensitive room temperature co2 gas sensor based on sno2-rgo hybrid composite. *Materials (Basel).* **2021**, *14*, 1–16, doi:10.3390/ma14030522.
21. Yuan, J.; Zhang, J.-J.; Yang, M.-P.; Meng, W.-J.; Wang, H.; Lu, J.-X. CuO Nanoparticles Supported on TiO2 with High Efficiency for CO2 Electrochemical Reduction to Ethanol. *Catalysts* **2018**, *8*, 171, doi:10.3390/catal8040171.
22. Bhuvaneshwari, S.; Gopalakrishnan, N. Facile synthesis of low dimensional CuO nanostructures and their gas sensing applications. *Cryst. Res. Technol.* **2016**, *51*, 145–153, doi:10.1002/crat.201500243.
23. Purushothaman, K.K.; Saravanakumar, B.; Babu, I.M.; Sethuraman, B.; Muralidharan, G. Nanostructured CuO/reduced graphene oxide composite for hybrid supercapacitors. *RSC Adv.* **2014**, *4*, 23485–23491, doi:10.1039/c4ra02107j.
24. Nagaraja, M.; Prashanth, S.; Pattar, J.; Mahesh, H.M.; Rajanna, K. Polyaniline-CuO nanocomposite: Electrical, structural and sensor properties. *Mater. Today Proc.* **2021**, 1–4, doi:10.1016/j.matpr.2021.08.154.
25. Kumar, P.; Kang, C.H.; Burhanudin, Z.A.; Saheed, M.S.M.; Irshad, M.I.; Mohamed, N.M. Graphene-based hybrid thin films as transparent conductive electrode for optoelectronic devices. In Proceedings of the IEEE International Conference on Semiconductor Electronics, Proceedings, ICSE; 2016; Vol. 2016-Septe, pp. 216–219.
26. Mandayo, G.G.; González, F.; Rivas, I.; Ayerdi, I.; Herrán, J. BaTiO3-CuO sputtered thin film for carbon dioxide detection. *Sensors Actuators, B Chem.* **2006**, *118*, 305–310.
27. Yoon, H.J.; Jun, D.H.; Yang, J.H.; Zhou, Z.; Yang, S.S.; Cheng, M.M.C. Carbon dioxide gas sensor using a graphene sheet. *Sensors Actuators, B Chem.* **2011**, *157*, 310–313, doi:10.1016/j.snb.2011.03.035.
28. Macinnes, M.M.; Hlynchuk, S.; Acharya, S.; Lehnert, N.; Maldonado, S. Reduction of Graphene Oxide Thin Films by Cobaltocene and Decamethylcobaltocene. *ACS Appl. Mater. Interfaces* **2018**, *10*, 2004–2015, doi:10.1021/acsami.7b15599.
29. Lesiak, B.; Trykowski, G.; Tóth, J.; Biniak, S.; Kövér, L.; Rangam, N.; Stobinski, L.; Malolepszy, A. Chemical and structural properties of reduced graphene oxide—dependence on the reducing agent. *J. Mater. Sci.* **2021**, *56*, 3738–3754, doi:10.1007/s10853-020-05461-1.
30. Ayesh, A.I.; Ahmed, R.E.; Al-Rashid, M.A.; Alarrouqi, R.A.; Saleh, B.; Abdulrehman, T.; Haik, Y.; Al-Sulaiti, L.A. Selective gas sensors using graphene and CuO nanorods. *Sensors Actuators, A Phys.* **2018**, *283*, 107–112, doi:10.1016/j.sna.2018.09.068.
31. Guo, L.; Hao, Y.W.; Li, P.L.; Song, J.F.; Yang, R.Z.; Fu, X.Y.; Xie, S.Y.; Zhao, J.; Zhang, Y.L. Improved NO2 Gas Sensing Properties of Graphene Oxide Reduced by Two-beam-laser Interference. *Sci. Rep.* **2018**, *8*, 1–7.
32. Sharma, B.; Kim, J.S. MEMS based highly sensitive dual FET gas sensor using graphene decorated Pd-Ag alloy nanoparticles for H2 detection. *Sci. Rep.* **2018**, *8*, 1–9, doi:10.1038/s41598-018-24324-z.
33. Hu, N.; Yang, Z.; Wang, Y.; Zhang, L.; Wang, Y. Ultrafast and sensitive room temperature NH 3 gas sensors based on chemically reduced graphene oxide. **2013**, doi:10.1088/0957-4484/25/2/025502.
34. Gupta, M.; Hawari, H.F.; Kumar, P.; Burhanudin, Z.A.; Tansu, N. Functionalized reduced graphene oxide thin films for ultrahigh co2 gas sensing performance at room temperature. *Nanomaterials* **2021**, *11*, 1–18, doi:10.3390/nano11030623.
35. Yang, H.; Li, J.S.; Zeng, X. Correlation between molecular structure and interfacial properties of edge or basal plane modified graphene oxide. *ACS Appl. Nano Mater.* **2018**, *1*, 2763–2773.
36. Kwan, Y.C.G.; Ng, G.M.; Huan, C.H.A. Identification of functional groups and determination of carboxyl formation temperature in graphene oxide using the XPS O 1s spectrum. *Thin Solid Films* **2015**, *590*, 40–48.
37. Zhang, D.; Jiang, C.; Liu, J.; Cao, Y. Investigation of CO2 reaction with copper oxide nanoparticles for room temperature gas sensing. *Sensors Actuators B Chem.* **2017**, *247*, 875–882, doi:10.1016/j.snb.2017.03.108.
38. Singh, P.; Nath, P.; Arun, R.K.; Mandal, S.; Chanda, N. Novel synthesis of a mixed Cu/CuO-reduced graphene oxide nanocomposite with enhanced peroxidase-like catalytic activity for easy detection of glutathione in solution and using a paper strip. *RSC Adv.* **2016**, *6*, 92729–92738.
39. Tang, Q.; Zhou, Z.; Chen, Z. Graphene-related nanomaterials: Tuning properties by functionalization. *Nanoscale* **2013**, *5*, 4541–4583, doi:10.1039/c3nr33218g.
40. Zhang, Q.; Pang, X.; Zhao, Y. Effect of the external velocity on the exfoliation properties of graphene from amorphous SiO2 surface. *Crystals* **2021**, *11*, doi:10.3390/cryst11040454.
41. Bhaumik, A.; Haque, A.; Taufique, M.; Karnati, P.; Patel, R.; Nath, M.; Ghosh, K. Reduced Graphene Oxide Thin Films with Very Large Charge Carrier Mobility Using Pulsed Laser Deposition. *J. Mater. Sci. Eng.* **2017**, *06*.
42. Li, Z.; Liu, Y.; Guo, D.; Guo, J.; Su, Y. Room-temperature synthesis of CuO/reduced graphene oxide nanohybrids for high-performance NO2 gas sensor. *Sensors Actuators, B Chem.* **2018**, *271*, 306–310, doi:10.1016/j.snb.2018.05.097.
43. Wu, J. Bin; Lin, M.L.; Cong, X.; Liu, H.N.; Tan, P.H. Raman spectroscopy of graphene-based materials and its applications in related devices. *Chem. Soc. Rev.* **2018**, *47*, 1822–1873, doi:10.1039/c6cs00915h.
44. Kumar, P.; Lin, K.; Seng, W.; Shuaib, M.; Saheed, M. Hybrid film of single-layer graphene and carbon nanotube as transparent conductive electrode for organic light emitting diode. *Synth. Met.* **2019**, *257*.

45. Cheng, C.; Zhang, C.; Gao, X.; Zhuang, Z.; Du, C.; Chen, W. 3D Network and 2D Paper of Reduced Graphene Oxide/Cu2O Composite for Electrochemical Sensing of Hydrogen Peroxide. *Anal. Chem.* **2018**, *90*, 1983–1991, doi:10.1021/acs.analchem.7b04070.
46. Muzyka, R.; Drewniak, S.; Pustelny, T.; Chrubasik, M.; Gryglewicz, G. Characterization of graphite oxide and reduced graphene oxide obtained from different graphite precursors and oxidized by different methods using Raman spectroscopy. *Materials (Basel).* **2018**, *11*, 15–17, doi:10.3390/ma11071050.
47. Wu, S.; Wan, L.; Wei, L.; Talwar, D.N.; He, K.; Feng, Z. Temperature-dependent optical properties of graphene on Si and SiO2/Si substrates. *Crystals* **2021**, *11*, doi:10.3390/cryst11040358.
48. Zaki, S.E.; Basyooni, M.A.; Shaban, M.; Rabia, M.; Eker, Y.R.; Attia, G.F.; Yilmaz, M.; Ahmed, A.M. Role of oxygen vacancies in vanadium oxide and oxygen functional groups in graphene oxide for room temperature CO2 gas sensors. *Sensors Actuators, A Phys.* **2019**, *294*, 17–24.